HHS Public Access

Author manuscript

Opt Lett. Author manuscript; available in PMC 2014 September 11.

Published in final edited form as:

Opt Lett. 2014 September 1; 39(17): 5192–5195.

Near-infrared Optical-resolution Photoacoustic Microscopy

Pengfei Hai[#], **Junjie Yao**[#], **Konstantin I. Maslov**, **Yong Zhou**, and **Lihong V. Wang**[*]

Optical Imaging Laboratory, Department of Biomedical Engineering, Washington University in St. Louis, One Brookings Drive, St. Louis, Missouri 63130, USA

[#] These authors contributed equally to this work.

Abstract

Compared with visible light (380–700 nm), near-infrared light (700–1400 nm) undergoes weaker optical attenuation in biological tissue, thus it can penetrate deeper. Here, we demonstrate near-infrared optical-resolution photoacoustic microscopy (NIR-OR-PAM) with 1046 nm illumination. A penetration depth of 3.2 mm was achieved in chicken breast tissue *ex vivo* using optical fluence within the ANSI limit (100 mJ/cm^2). Beyond ~0.6 mm deep in chicken breast tissue, NIR-OR-PAM has shown finer resolution than the visible counterpart with 570 nm illumination. The deep imaging capability of NIR-OR-PAM was validated in both the mouse ear and mouse brain. NIR-OR-PAM of possible lipid contrast was explored as well.

With 100% sensitivity to optical absorption, optical-resolution photoacoustic microscopy (OR-PAM) can provide both anatomical and functional information with high spatial resolution [1-5]. In OR-PAM, the high lateral resolution is achieved by tightly focusing the laser beam into a diffraction-limited spot [6]. In a highly scattering medium such as biological tissue, the focusing capability of OR-PAM degrades with the imaging depth [7]. In previous OR-PAM studies, ultraviolet (UV) or visible (VIS) light was used for illumination, mainly because of the strong absorption of DNA/RNA, cytochromes, hemoglobin, and melanin in these wavelength regions [8-9]. However, the strong optical scattering limits the penetration depth of OR-PAM in biological tissue.

To improve the imaging depth, we propose near-infrared (NIR) OR-PAM. Compared with visible illumination, NIR illumination yields several benefits. First, NIR-OR-PAM can penetrate deeper in tissue for a given signal-to-noise ratio (SNR), primarily due to weaker absorption of NIR light by blood [10]. Second, with weaker scattering of NIR light, NIR-OR-PAM can maintain its lateral resolution at greater depths. Third, NIR-OR-PAM can image other tissue components, such as water and lipid [11-12]. The optical absorption spectra of four tissue components from 250 nm to 1150 nm are shown in Fig. 1(a) [13-14]. Fourth, the American National Standard Institute (ANSI) permits stronger NIR light intensity on the tissue surface [15]. Here, we applied NIR light in OR-PAM and demonstrated these advantages.

[*]Corresponding author: lhwang@wustl.edu.

OCIS Codes: (110.3080) Infrared imaging; (170.5120) Photoacoustic imaging; (180.0180) Microscopy.

In the NIR-OR-PAM system [Fig. 1(b)], a Nd:YLF laser (INNOSAB, Edgewave, GmbH) generates laser pulses at its fundamental wavelength of 1046 nm. The laser pulses then pass through a second harmonic generator to generate 523 nm laser pulses. After the second harmonic generator, 523 nm and residual 1046 nm laser beams are split by a dichroic mirror. A dye laser (CBR-D, Sirah, GmbH) is pumped by the 523 nm beam and emits laser pulses with tunable wavelengths. We selected 570 nm for photoacoustic (PA) imaging, referred as VIS-OR-PAM, to compare with NIR-OR-PAM. A flip mirror is used to select either the 570 nm or the 1046 nm laser beam. After this, the laser beam is reshaped by an iris (ID25SS, Thorlabs) and then attenuated by a neutral density filter (NDC-50C-2M, Thorlabs). A condenser lens (LA1131, Thorlabs) and a 50 μm diameter pinhole (P50C, Thorlabs) spatially filter the beam further. The laser beam is then focused into the sample by an objective (AC127-050-A, Thorlabs; numerical aperture: 0.1 in air). A high-frequency ultrasonic transducer is placed confocally with the objective to detect the generated PA waves. The acoustic-optical coaxial alignment is achieved by using a beam combiner composed of a thin layer of silicone oil sandwiched between a right-angle prism (NT32-545, Edmund Optics) and a rhomboid prism (NT49-419, Edmund Optics). Each laser pulse generates a one-dimensional PA image (A-line) by recording the time course of the PA signal. Volumetric imaging is provided by two dimensional motor scanning.

To measure the penetration depth of the NIR-OR-PAM, we imaged a 50 μm diameter black human hair obliquely inserted into a piece of fresh chicken breast tissue. To conform to the ANSI safety limit [15], the light fluences on the tissue surface at 570 nm and 1046 nm were adjusted to 20 mJ/cm^2 and 100 mJ/cm^2, respectively. NIR-OR-PAM was able to image the black hair 3.2 mm beneath the skin surface with an SNR of 6 dB compared to only 2.3 mm by VIS-OR-PAM with the same SNR [Figs. 2(a) and 2(b)]. NIR-OR-PAM can penetrate deeper than VIS-OR-PAM: First, NIR light undergoes weaker optical attenuation than VIS light, which allows it to penetrate deeper; Second, ANSI permits stronger NIR light fluence on tissue surface, which also gives us larger penetration depth. The same time-gain compensation (TGC, 0.75 dB/MHz/cm) for acoustic attenuation was applied to improve the visibility in both cases.

To measure the lateral resolution of the NIR-OR-PAM system in clear media, a sharp metal edge was imaged with a step size of 0.625 μm and a scanning range of 100 μm along the x-axis. By fitting the measured data to an edge spread function, the full width at half maximum (FWHM) of the corresponding line spread function was estimated as the lateral resolution. The lateral resolution of NIR-OR-PAM in a clear medium was estimated to be 6.2 μm [Fig. 3(b)], and that of VIS-OR-PAM was estimated to be 2.9 μm [Fig. 3(a)], both of which are close to the theoretical lateral resolutions of OR-PAM, which are determined by the focal diameters of the laser beams. The axial resolution of NIR-OR-PAM was estimated to be ~27 μm, based on the transducer bandwidth and the speed of sound in tissue [16]. In scattering media such as biological tissue, both the lateral and axial resolutions decrease with imaging depth due to optical scattering and frequency-dependent acoustic attenuation in tissue.

The lateral resolutions of NIR-OR-PAM and VIS-OR-PAM at different imaging depths were measured in scattering media. A sharp metal edge obliquely inserted into a piece of

fresh chicken breast tissue was imaged at different depths while the optical focus was maintained on the metal edge. As optical focusing deteriorated in tissue, the line spread functions were no longer Gaussian functions [7], thus the lateral resolution could no longer be estimated by fitting the edge spread functions using error functions, as we did for the clear medium. Therefore, we estimated the lateral resolution as the FWHM of the numerical first-derivative of the measured edge spread function. Fig. 3(c) shows the lateral resolutions of both NIR-OR-PAM and VIS-OR-PAM as functions of imaging depth. Due to optical scattering in the chicken tissue, the optical focusing degrades with depth, deteriorating the lateral resolution of OR-PAM. At 1046 nm, scattering in chicken breast tissue is weaker than that at 570 nm. With weaker optical scattering, NIR light can focus better than VIS light after traveling through a certain depth, which results in finer lateral resolution in NIR-OR-PAM over VIS-OR-PAM. For VIS-OR-PAM, the lateral resolution is finer than 40 μm up to ~1.6 mm depth, while for NIR-ORPAM the lateral resolution is finer than 40 μm up to ~2 mm depth. Close to the tissue surface (<0.6 mm), NIR-OR-PAM has a worse lateral resolution than VIS-OR-PAM due to the longer wavelength; at ~0.6 mm depth, NIR-OR-PAM and VIS-OR-PAM show similar resolutions. As the imaging depth goes beyond 0.6 mm, NIR-OR-PAM has finer lateral resolutions than VIS-OR-PAM, until the optical focusing becomes so ineffective that OR-PAM turns into acoustic-resolution PAM, where the acoustic focusing of the 50 MHz ultrasonic transducer (~43 μm) determines the lateral resolution.

A mouse ear was imaged in vivo with NIR-OR-PAM. All experimental animal procedures were carried out in conformity with the laboratory animal protocol approved by the Animal Studies Committee at Washington University in St. Louis. A 2×2 mm^2 area of the mouse ear was imaged by both VIS-OR-PAM and NIR-OR-PAM [Figs. 4(a) and 4(b)]. VIS-OR-PAM is able to image only the blood vessels [Fig. 4(a)]. NIR-OR-PAM, however, is able to image more contrasts [Fig. 4(b)]. In addition to blood vessels, the circular structures imaged by NIR-ORPAM are suspected to be fat cells surrounding sebaceous glands [17-18]. Close-up images and B-scan images [Figs. 4(c) and 4(d)] further demonstrate the improvement of NIR-OR-PAM in lipid contrast and imaging depth in vivo.

We also imaged a mouse brain in vivo with NIR-OR-PAM. The same area of the mouse brain was imaged by VIS-OR-PAM and NIR-OR-PAM. The scalp was removed but the skull was intact. Due to the strong blood absorption and brain tissue scattering, few blood vessels deeper than 0.5 mm can be imaged by VIS-OR-PAM [Figs. 5(a) and 5(b)]. However, NIR-OR-PAM can detect signals from blood vessels deeper than 0.5 mm [Figs. 5(c) and 5(d)].

NIR-OR-PAM can not only penetrate deeper than VIS-OR-PAM but also image structures in deep regions with finer resolution. As shown in Figs. 6(a) and 6(b), at both illumination wavelengths, OR-PAM was able to clearly image the cortical vascular network. However, close-ups of the vessels more than 200 μm deep in Figs. 6(a) and 6(b) show that the vessels are less blurred in the NIR-OR-PAM images than in the VIS-OR-PAM images, as shown in Fig. 6(c). The lateral resolution improvement for in vivo imaging by NIR-OR-PAM was estimated by comparing the apparent diameters of vessels at the same depths. The apparent diameters of two representative vessels were 120 μm and 160 μm in VIS-OR-PAM, while

they were 50 μm and 80 μm in NIR-OR-PAM, respectively [Fig. 6(d)]. The apparent diameters of blood vessels were ~2 times smaller in NIR-OR-PAM.

Due to strong absorption, an overlying blood vessel may shadow vessels underneath in VIS-OR-PAM. At 1046 nm, the optical absorption of hemoglobin is about 40 times less than that at 570 nm [Fig. 1(a)]. Therefore, 1046 nm NIR light has a 1/e penetration depth of 1.2 mm in blood, and is able to image multiple layers of blood vessels. This advantage was demonstrated by imaging a bleeding area in a mouse brain. The bleeding layer appears weaker in NIR-OR-PAM than in VIS-OR-PAM [Figs. 7(a) and 7(b)]. By peeling off the bleeding layer in data processing, we can clearly see that the optical shadowing from the bleeding layer is weaker in NIR-OR-PAM, and the vascular network underneath can thus be better resolved with greater SNR. However, due to the strong absorption, nearly all of the VIS light is absorbed by the blood pool, and generated strong PA signals that were reverberated by other underlying brain structures, showing as a ‘ghost’ image of the blood pool.

It is worth pointing out that lower optical absorption in the NIR region allows deeper penetration but results in weaker PA signals. However, with nanosecond pulse excitation, the tissue damage mechanism is mainly photothermal [19]. Therefore, lower absorption allows for stronger excitation fluence, which can partially compensate for the reduced signal strength.

In conclusion, we have demonstrated that NIR-OR-PAM offers new imaging contrast and better resolution at deeper imaging depths than VIS-OR-PAM. By employing NIR light with our fast-scanning OR-PAM [20] and incorporating multiple wavelengths [21], we should be able to measure hemodynamic parameters, including blood flow speed, the oxygen saturation of hemoglobin, and the metabolic rate of oxygen [22].

Acknowledgments

The authors appreciate Prof. James Ballard’s close reading of the manuscript. This work was sponsored by NIH grants DP1 EB016986 (NIH Director’s Pioneer Award), R01 CA186567 (NIH Director’s Transformative Research Award), and R01 CA159959, and NSF grant 1255930. L.W. has a financial interest in Microphotoacoustics, Inc. and Endra, Inc., which, however, did not support this work. K. M. has a financial interest in Microphotoacoustics, Inc.

References

1. Wang LV, Hu S. Photoacoustic tomography: *in vivo* imaging from organelles to organs. Science. 2012; 335:1458–1462. [PubMed: 22442475]
2. Yao J, Wang LV. Photoacoustic microscopy. Laser & Photonics Reviews. 2013; 7:758–778.
3. Yao J, Wang L, Li C, Zhang C, Wang LV. Photoimprint photoacoustic microscopy for three-dimensional label-free subdiffraction imaging. Phys. Rev. Lett. 2014; 112:014302. [PubMed: 24483902]
4. Liang J, Zhou Y, Maslov KI, Wang LV. Cross-correlation-based transverse flow measurements using optical resolution photoacoustic microscopy with a digital micro mirror device. J. Biomed. Opt. 2013; 18:096004. [PubMed: 24002191]
5. Paproski RJ, Forbrich AE, Wachowicz K, Hitt MM, Zemp RJ. Tyrosinase as a dual reporter gene for both photoacoustic and magnetic resonance imaging. Biomed. Opt. Express. 2011; 2:771–780. [PubMed: 21483602]

6. Maslov K, Zhang HF, Hu S, Wang LV. Optical-resolution photoacoustic microscopy for *in vivo* imaging of single capillaries. Opt. Lett. 2008; 33:929–931. [PubMed: 18451942]
7. Liu Y, Zhang C, Wang LV. Effects of light scattering on optical-resolution photoacoustic microscopy. J. Biomed. Opt. 2011; 17:126014. [PubMed: 23232794]
8. Xie Z, Chen S, Ling T, Guo LJ, Carson PL, Wang X. Pure optical photoacoustic microscopy. Opt. Express. 2011; 19:9027–9034. [PubMed: 21643156]
9. Zhang C, Zhang Y, Yao DK, Xia Y, Wang LV. Label-free photoacoustic microscopy of cytochromes. J. Biomed. Opt. 2013; 18:020504.
10. Homan K, Kim S, Chen Y-S, Wang B, Mallidi S, Emelianov S. Prospects of molecular photoacoustic imaging at 1064 nm wavelength. Opt. Lett. 2010; 35:2663–2665. [PubMed: 20680092]
11. Xu Z, Li CH, Wang LV. Photoacoustic tomography of water in phantoms and tissue. J. Biomed. Opt. 2010; 15:036019. [PubMed: 20615021]
12. Allen TJ, Hall A, Dhillon AP, Owen JS, Beard PC. Spectroscopic photoacoustic imaging of lipid-rich plaques in the human aorta in the 740 to 1400 nm wavelength range. J. Biomed. Opt. 2012; 17:061209. [PubMed: 22734739]
13. van Veen RLP, Sterenborg HJCM, Pifferi A, Torricelli A, Cubeddu R. Determination of VIS-NIR absorption coefficients of mammalian fat, with time- and spatially resolved diffuse reflectance and transmission spectroscopy. Biomedical Topical Meeting, OSA Technical Digest. 2004 paper SF4.
14. Hale GM, Querry MR. Optical constants of water in the 200 nm to 200 μm wavelength region. Appl. Opt. 1973; 12:555–563. [PubMed: 20125343]
15. American National Standards Institute (ANSI). American national standard for the safe use of lasers. Standard. 2007 Z136.1–2007.
16. Wang L, Maslov K, Yao J, Rao B, Wang LV. Fast voice-coil scanning optical-resolution photoacoustic microscopy. Opt. Lett. 2011; 36:139–141. [PubMed: 21263479]
17. Freudiger CW, Min W, Saar BG, Lu S, Holtom GR, He C, Tsai JC, Kang JX, Xie XS. Label-Free biomedical imaging with high sensitivity by stimulated Raman scattering microscopy. Science. 2008; 322:1857–1861. [PubMed: 19095943]
18. Matthews T, Zhang C, Yao D, Maslov K, Wang LV. Label-free photoacoustic microscopy of peripheral nerves. J. Biomed. Opt. 2014; 19:016004.
19. Sato S, Ogura M, Ishihara M, Kawauchi S, Arai T, Matsui T, Kurita A, Obara M, Kikuchi M, Ashida H. Nanosecond, high-intensity pulsed laser ablation of myocardium tissue at the ultraviolet, visible, and near-infrared wavelengths: in-vitro study. Lasers. Surg. Med. 2001; 29:464–473. [PubMed: 11891735]
20. Yao J, Huang CH, Wang L, Yang JM, Gao L, Maslov KI, Zou J, Wang LV. Wide-field fast-scanning photoacoustic microscopy based on a water-immersible MEMS scanning mirror. J. Biomed. Opt. 2012; 17:0805051.
21. Zhang HF, Maslov K, Stoica G, Wang LV. Functional photoacoustic microscopy for high-resolution and noninvasive *in vivo* imaging. Nature biotechnology. 2006; 24:848–851.
22. Yao J, Maslov KI, Zhang Y, Xia Y, Wang LV. Label-free oxygen-metabolic photoacoustic microscopy *in vivo*. J. Biomed. Opt. 2011; 16:076003. [PubMed: 21806264]

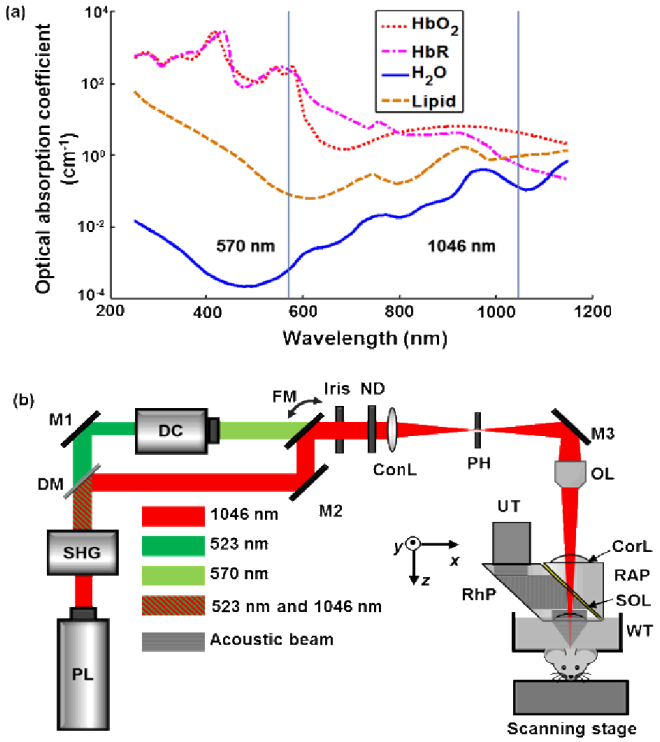

Fig. 1.

Absorption spectra of four tissue components and the schematic of NIR-OR-PAM. (a) Absorption spectra of oxyhemoglobin (HbO_2) (150 g/L or 2.3 mM in blood), deoxyhemoglobin (HbR) (150 g/L or 2.3 mM in blood), water (80% by volume in tissue), and lipid (20% by volume in tissue) from 250 nm to 1150 nm. (b) Schematic of the NIR-OR-PAM system. ConL, condenser lens; CorL, correction lens; DC, dye cell; DM, dichroic mirror; FM, flip mirror; M1, M2, and M3, mirrors; ND, neutral density filter; OL, objective lens; PH, pinhole; PL, pump laser; RAP, right-angle prism; RhP, rhomboid prism; SHG, second harmonic generator; SOL, silicone oil layer; UT, ultrasonic transducer; WT, water tank.

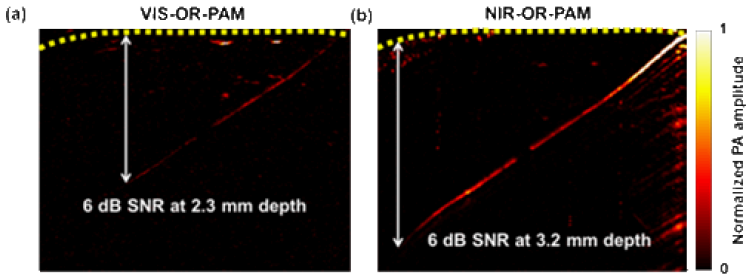

Fig. 2.

Penetration depths of the two OR-PAM systems. VIS-ORPAM (a) and NIR-OR-PAM (b) images of a black human hair inserted obliquely into a piece of fresh chicken breast tissue. The hair was imaged with an SNR of ≥ 6 dB up to 3.2 mm deep in the tissue by NIR-OR-PAM and 2.3 mm deep in the tissue by VIS-OR-PAM.

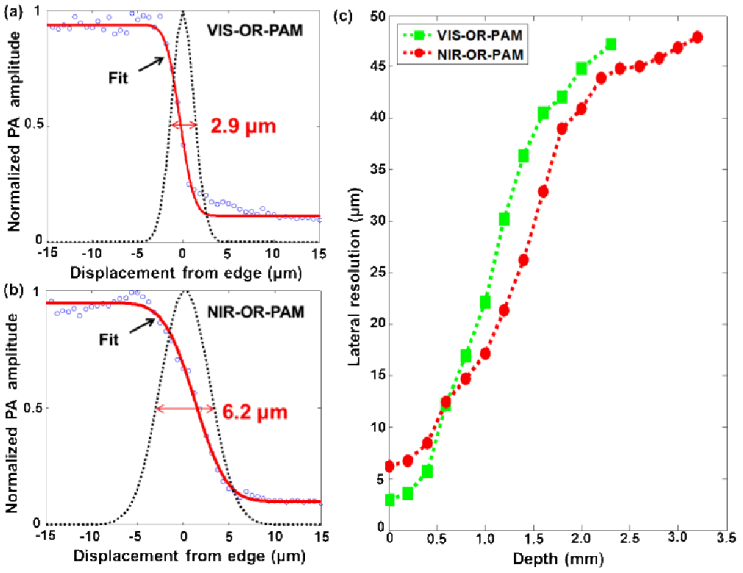

Fig. 3.

Lateral resolutions of the two OR-PAM systems. (a-b) Line spread functions (black dotted lines) extracted from the fitted edge spread functions (solid red lines) of VIS-OR-PAM (a) and NIR-OR-PAM (b) acquired in water. Here, the lateral resolution was quantified as the FWHM of the line spread functions. The lateral resolution of NIR-OR-PAM in water is 6.2 μm, while the lateral resolution of VIS-OR-PAM is 2.9 μm. (c) Lateral resolution of NIR-OR-PAM and VIS-OR-PAM as a function of imaging depth in scattering media. Here, the lateral resolution was quantified as the FWHM of the numerical first-derivative of the measured edge spread function.

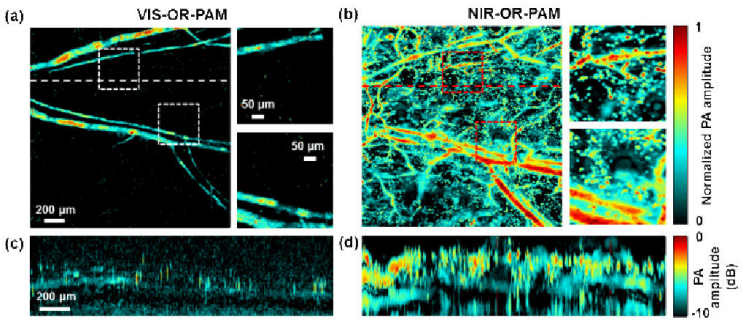

Fig. 4.

Comparison of images of a mouse ear acquired using visible and NIR light in vivo. (a) A maximum amplitude projection (MAP) image of a mouse ear acquired by VIS-OR-PAM in vivo within depths up to 300 μm. Two close-ups show the PA signals from blood vessels, as indicated by the dashed boxes. (b) An MAP image of the same mouse ear acquired by NIR-OR-PAM in vivo within depths up to 300 μm. (c-d) B-scan images along the dashed lines in (a) and (b), respectively, on a logarithmic scale after acoustic attenuation compensation with an acoustic attenuation coefficient of 1 dB/MHz/cm.

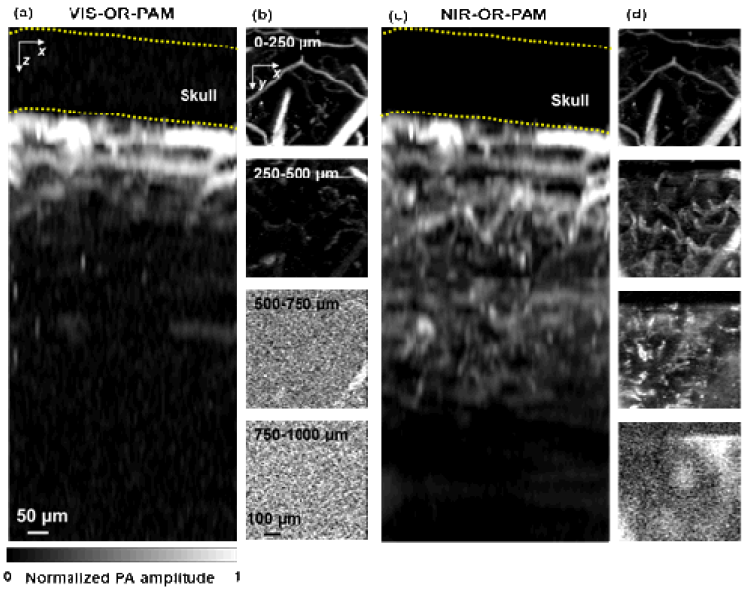

Fig. 5.

Comparison of in vivo imaging depths in a mouse brain. (a) x-z projection of a VIS-OR-PAM image of the mouse brain acquired in vivo. (b) x-y projections of the mouse brain at different depths. No structure can be detected at depths beyond 500 μm. (c) x-z projection of a NIR-OR-PAM image of the same mouse brain acquired in vivo. (d) x-y projections of the mouse brain at different depths. Structures can be detected at depths up to 750 μm. The dashed lines in the x-z projections mark the approximate location of the skull.

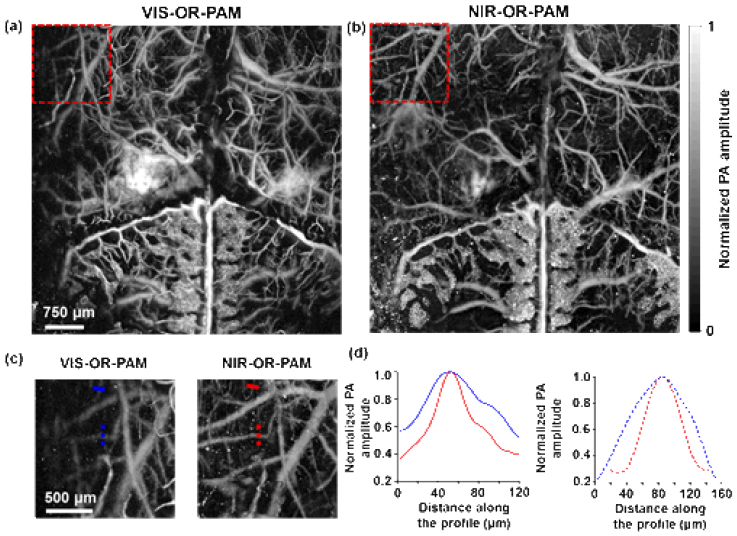

Fig. 6.

Comparison of in vivo lateral resolutions in mouse brain. (a-b) In vivo mouse brain MAP images acquired by VIS-OR-PAM (a) and NIR-OR-PAM (b), respectively. (c) Close-ups of the dashed boxes in (a) and (b) show that more blood vessels can be imaged by NIR-OR-PAM. (d) Normalized PA amplitudes across two selected blood vessels at 225 μm (solid lines) and 330 μm (dashed lines) depths in (c), respectively. Both vessels have smaller apparent diameters in the NIR-OR-PAM image than in the VIS-OR-PAM image, because they are less blurred.

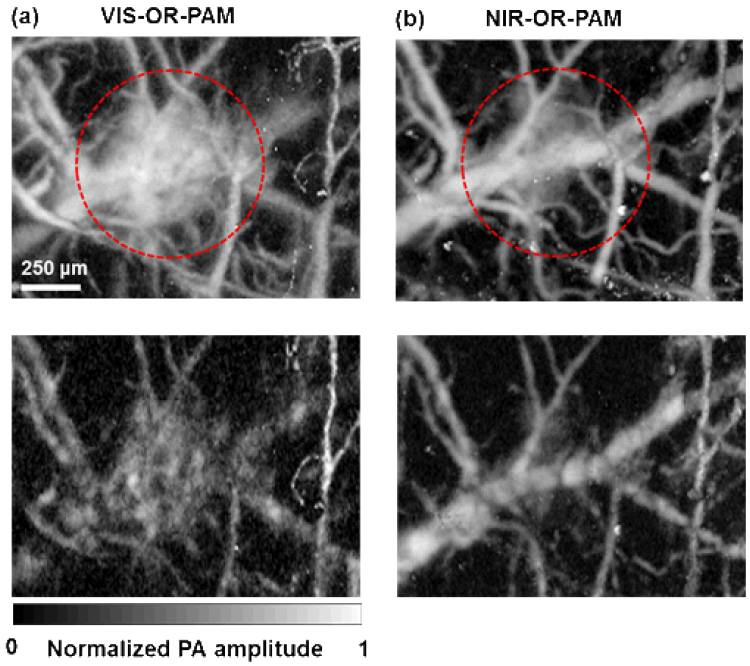

Fig. 7.

Comparison of penetrations in blood. (a) Top: a VIS-ORPAM MAP image of a mouse brain acquired in vivo within depths up to 300 μm, in which blood vessels were covered by a bleeding layer. Bottom: a VIS-OR-PAM MAP image of the same area in the mouse brain acquired in vivo within depths from 100 μm to 300 μm after digitally peeling off the bleeding layer. The underneath blood vessels can barely be resolved. (b) Top: an NIROR-PAM MAP image of the same region as (a) within depths up to 300 μm. The signal strength from the bleeding layer is weaker than that from the VIS-OR-PAM counterpart. Bottom: an NIROR-PAM MAP image of the same area in the mouse brain acquired in vivo within depths from 100 μm to 300 μm after digitally peeling off the bleeding layer. The underneath blood vessels can be clearly resolved.